Decision Support in Peripheral Arterial Occlusive Disease Management with AI-Enhanced Super-Resolution Techniques for Advanced Vascular Imaging

Alexandra La Cruz[0000−0001−6052−2933],
Juan Pedro Felipe,
Erika Severeyn[0000−0002−9500−3532], and
Andrés García-León[0000−0003−1757−6885]

Abstract Peripheral Arterial Occlusive Disease (PAOD) management is essential in combating atherosclerosis-induced blockages, requiring advanced vascular imaging for accurate diagnosis and treatment. Artificial intelligence-enhanced super-resolution (SR) techniques are increasingly recognized for improving vascular imaging and decision support, enhancing PAOD treatment accuracy and efficacy. PAOD, caused by atherosclerosis, reduces blood flow to the lower extremities. Computed tomography angiography (CTA) images are used for evaluating PAOD, offering detailed visualization of vascular structures. This study used CTA images, the most common modality for daily PAOD evaluation, to demonstrate the role of SR techniques in decision support systems, particularly in healthcare. The research addresses challenges in segmenting CTA images of lower extremity arteries, highlighting SR techniques' potential in refining artery segmentation, 3-D modeling, and visualization. Comparing SR models like SRCNN, EDSR, RCAN, SRGAN, and ESRGAN, the study identifies SRGAN as the optimal choice. These are models based on deep learning and generative models. Metrics like peak signal-to-noise ratio (PSNR) and structural similarity (SSIM) validate model efficacy. This sophisticated technology aids healthcare professionals in making smarter decisions, analyzing complex information, and providing valuable recommendations.

Alexandra La Cruz

Faculty of Engineering, Universidad de Ibagué, Ibagué, Tolima, Colombia, e-mail: alexandra.lacruz@unibague.edu.co

Juan Pedro Felipe

Computer Engineer and Biomedical Engineering, Universidad Internacional de Valencia, Valencia, España, e-mail: Felipe@gmail.com

Erika Severeyn

Department of Thermodynamics and Transfer Phenomena, Universidad Simón Bolívar, Venezuela, e-mail: severeynerika@usb.ve

Andrés García-León

Tecnológico de Monterrey, Escuela de Ingeniería y Ciencias, e-mail: andres.garcialeon@tec.mx

1 Introduction

Different epidemiological studies have shown that up to 50% of patients with the PAOD [3] have symptoms of cerebrovascular or cardiological disease, a real cause of patient morbidity and mortality [21]. PAOD describes a narrowing (stenosis) or complete blockage (occlusion) of the arteries of the arm or leg (see Fig. 1) [3]. PAOD can cause leg pain when walking (intermittent claudication), which may go away with rest. Over time, the disease can worsen and there may be pain even at rest, leg ulcers, and, in severe cases, gangrene, which may lead to amputation of the affected limb [3]. Consequently, in patients with PAOD, atherosclerotic stenosis is likely to appear in other areas of the body, such as in the coronary arteries and cerebral arteries. Mortality and morbidity caused by PAOD will depend largely on poor circulation in these areas rather than on limb ischemia [3, 1].
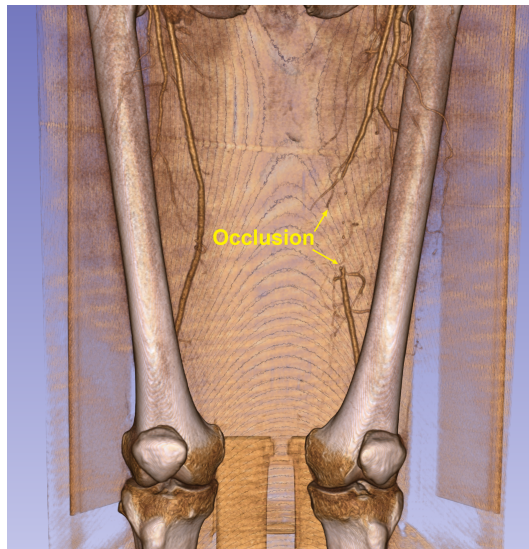
Fig. 1 3-D visualization of a PAOD case of a patient. The arrows indicate the begin-ends of the occlusion.

Advanced imaging techniques like computed tomography angiography (CTA), magnetic resonance angiography (MRA), and duplex ultrasound are key to visualizing vascular structures in PAOD patients [19]. These methods allow detailed assessment of arterial narrowing or blockages, essential for treatment planning. This study uses CTA images, the most common modality for PAOD evaluation. Three-dimensional (3-D) reconstruction from CTA images helps visualize arteries, including stenosis or occlusion, aiding interventions like angioplasty or bypass surgery [23, 34]. SR techniques enhance 3-D models, particularly in areas with small blood vessels, where traditional methods like interpolation struggle with low-resolution images. Despite challenges in data acquisition and processing, 3-D rendering improves PAOD assessment by providing accurate anatomical details

and supporting collaborative decision-making [18]. Beyond PAOD, 3-D modeling is useful in surgical planning and augmented reality applications [29].

Small blood vessel diameters present significant challenges for 3-D rendering, requiring high spatial resolution through CTA or MRA for accurate detail capture. Noise reduction, advanced vessel segmentation, and SR techniques are essential for improving image quality. Visualizing small vessels affected by atherosclerosis remains difficult [15], as healthy arteries have uniform CT density, while diseased arteries show varying attenuation. Image noise, scanning artifacts, and arterial contrast variations complicate visualization. Despite these challenges, advances in imaging technology are improving 3-D rendering. Super-resolution techniques, particularly for low-resolution images, can significantly enhance the quality of 3-D models.

This chapter examines the impact of deep learning-based SR techniques on the diagnosis and care of PAOD patients through CTA image processing. Advanced SR techniques in CTA imaging are poised to improve diagnostic accuracy and treatment planning by offering precise 3-D visualizations. These techniques support clinicians with a robust decision support system (DSS). The models studied include SRCNN [5], EDSR [17], RCAN [32], SRGAN [25], and ESRGAN [30], adapted for CTA image processing. The chapter highlights how SR techniques can improve the visualization of small blood vessels in atherosclerotic patients, advancing medical diagnostics and decision support, ultimately enhancing patient care. The hypothesis is whether these models effectively enhance the resolution of vascular structures in the lower extremities.

The paper follows a structured approach with five key sections: (1) Section 3 provides a literature review and research context, (2) Section 4 details the methodology encompassing dataset and SR techniques, (3) Section 5 presents our findings, (4) Section 6 engages in an in-depth discussion of results and their relevance to existing knowledge, and concludes the paper while proposing future research.

2 Impact of including SR techniques in DSS in health-systems

Super-resolution (SR) techniques are crucial in Decision Support Systems (DSS) for medical imaging, enhancing the visualization of vascular structures in CTA images. These techniques improve image resolution, making small arteries clearer, which is vital for accurate diagnosis and treatment planning, especially in conditions like PAOD. SR helps reveal pathologies not visible in lower-resolution scans, improving diagnostic accuracy and enabling earlier interventions. Integrating SR into automated analysis workflows allows machine learning models to detect anomalies and assess vascular health, enhancing clinical decision-making. SR can be seamlessly incorporated into clinical imaging workflows, providing enhanced CTA images with minimal manual intervention. Optimized for real-time processing, SR algorithms support timely decision-making, especially during procedures like angiography. SR's integration into clinical environments can be facilitated through

user-friendly interfaces, improving workflow efficiency. By improving image quality, SR techniques reduce the need for repeat imaging, saving costs and minimizing patient exposure to radiation. Faster, more accurate diagnoses streamline the diagnostic process, enhance patient satisfaction, and lower operational costs. SR also optimizes resource use by allowing more efficient allocation of medical staff, ultimately improving patient outcomes and reducing long-term healthcare costs

3 Related Works

Single Image Super-Resolution (SISR) aims to increase the resolution of low-resolution images by restoring high-frequency information. Most SISR methods, like sparse coding [5], extract key features from the image and encode them into a low-resolution structure. This compact representation captures essential details while reducing data size. Sparse coefficients are then passed to a high-resolution dictionary to reconstruct the image. Traditional SR methods typically do not integrate generative models into a unified optimization framework, which is a key aspect of modern approaches. This research evaluates whether generative models effectively enhance the resolution of vascular structures in lower extremities.

Convolutional Neural Network (CNN)-based methods have greatly improved the performance of SISR [35]. Dong et al. pioneered the use of CNNs to solve the SISR problem in [35]. They showed that conventional sparse coding-based SR methods existing at the time can be reformulated into a deep CNN, achieving superior performance. This model is divided into three phases, each performed by a convolution: feature mapping, nonlinear feature mapping, and reconstruction to a high-resolution representation.

Dong et al. introduced the SRCNN, a deep learning technique that can reformulate the conventional sparse coding-based SR methods and achieve superior performance [5]. From that point on, numerous methods employing deep learning were developed to address the SR problem. Residual models such as Very Deep Convolutional Networks (VDCN) [13], Deeply-Recursive Convolutional Networks (DRCN) [14], and Deep Recursive Residual Network (DRRN) [26] emerged, building the neural network based on units or blocks that learn through residual functions, which represent the difference between the original and processed image. Residual networks can converge faster, requiring fewer epochs and providing a higher Peak Signal-to-Noise Ratio (PSNR) [12] in training, which quantitatively measures the quality of the image reconstruction.

Subsequently, some approaches employ a de-convolution layer at the end of the network that directly maps the original low-resolution image to the high-resolution image [6]. Some others approaches extract features from the low-resolution space and maps them to the high-resolution space [25]. These scaling techniques have been leveraged by several residual models, which use residual scaling methods to improve the stability and performance of deep networks. Alternatively, some models utilize a Residual Dense Block (RDB) as the central component in network construction,

where each RDB consists of densely connected layers and local feature fusion with local residual learning [33].

Recent advancements introduce the Generative Adversarial Networks (GAN) [9]. GAN models consist of a generator that produces SR images and a discriminator that evaluates whether the generated image is real or artificial. A good approximation of the high-resolution image is assumed if the discriminator cannot distinguish between the generated image and the original image [25]. In addition, a new function in GAN is used as a discriminator to enable the generator to retrieve more detailed textures by learning to infer which image is more realistic [30]. Furthermore, a residual-in-residual (RIR) structure has been proposed to address the low-frequency information removed through multiple hopping connections. This structure incorporates a Channel Attention (CA) mechanism that adaptively rescales channel characteristics by considering channel inter-dependencies [32].

In this paper we have divided SR-algorithms into several groups based on their network architectures and characteristics within the context of super-resolution techniques. The algorithms are categorized into four sets, each focusing on specific aspects of network design and methodology.

3.1 Residual-based models

Residual models focus on learning the difference between the input and desired output, simplifying the learning of identity mappings and aiding in the training of deeper networks. A well-known example of this approach is ResNet, which helps mitigate the vanishing gradient problem. Building on this, Very Deep Super-Resolution (VDSR) networks [13] utilize deep structures with small filters to efficiently capture contextual information across large image regions. By applying residual learning and high learning rates, they optimize the network quickly, ensuring training stability through gradient clipping. Expanding on these concepts, the Deep Recursive Convolutional Network (DRCN) [14] introduces up to 16 recursive layers, enhancing performance without increasing the number of parameters. This is achieved by using recursive supervision and skipping connections, which make training more manageable. Further advancing this idea, the Deep Recursive Residual Network (DRRN) [26] proposes a deeper model with up to 52 convolutional layers. By leveraging residual learning, it improves performance while using fewer parameters, building on the success of earlier models.

3.2 Scaling methods

Scaling models aim to enhance the network's capacity by increasing the number of layers, channels (width), or the resolution of input images. This approach is designed to boost the network's performance by enabling it to capture more complex patterns. Dong et al. further refined their SRCNN model for practical applications that require real-time performance (24 fps), achieving better quality and a 40-fold increase

in speed. Their proposed model, the Fast Super-Resolution Convolutional Neural Network (FSRCNN) [6], introduced three key improvements: first, it incorporates a de-convolution layer at the network's end, directly mapping the low-resolution image to its high-resolution counterpart; second, it reduces the input dimension by reformulating the mapping layer; and third, it uses smaller filters but more mapping layers, optimizing computational efficiency.

Building on this, the Efficient Sub-Pixel Convolutional Network (ESPCN) [25] introduces another innovation by extracting feature maps in the low-resolution space, eliminating the need to scale the input image to high resolution. This reduces the computational load while maintaining performance. Furthermore, it incorporates a sub-pixel convolutional layer that learns a set of filters to scale the final low-resolution feature map to a high-resolution output.

3.3 Integrating Residual and Scaling Methods for Enhanced Super-Resolution Performance

By combining scaling strategies with residual learning, models can achieve both high performance and computational efficiency. Residual connections allow networks to focus on learning high-frequency details, crucial for super-resolution, while scaling strategies (such as depth, width, and resolution) enhance the network's ability to capture finer details, improving the quality of super-resolved images. Models integrating residual learning with scaling methods represent a hybrid approach that leverages the strengths of both techniques. The residual component enables the network to capture fine details, while scaling methods optimize the network's capacity to enhance image resolution. Below are key models that integrate both approaches.

The Enhanced Deep Super-Resolution (EDSR)[17] model improves upon SRResNet by removing unnecessary modules to create a more compact and efficient architecture. By using residual scaling techniques, EDSR stabilizes the deep model and delivers superior performance, winning the NTIRE2017 SR Challenge[27]. The Laplacian Pyramid Super-Resolution Network (LapSRN) [16] reconstructs high-resolution images progressively through sub-band residuals. This model eliminates the need for bicubic interpolation, reducing computational complexity while using deep supervision and a robust loss function to ensure high-quality reconstruction. SRDenseNet [28] introduces dense hopping connections, where feature maps from each layer are propagated to all subsequent layers. This facilitates the combination of low-level and high-level features, improving reconstruction performance and mitigating the vanishing gradient problem in very deep networks. Additionally, de-convolution layers accelerate the up-sampling process. The Residual Dense Network (RDN) [33] addresses the challenge of inefficient use of hierarchical features in low-resolution images, which can limit performance in deep CNN-based SR models. RDN incorporates Residual Dense Blocks (RDBs) to efficiently fuse features and retain crucial information, enabling the network to scale effectively and stabilize during training.

Lastly, the Residual Channel Attention Network (RCAN) [32] introduces a Residual in Residual (RIR) structure that focuses the network on high-frequency information by removing low-frequency data. With its Channel Attention (CA) mechanism, RCAN adapts the network's focus on relevant channel characteristics by considering relationships across channels.

The Enhanced Deep Super-Resolution (EDSR) [17] residual network model was designed with an improvement of the SRResNet model, achieving better results by eliminating unnecessary modules while obtaining a more compact model. They used residual scaling techniques to give stability to the deep model. This method showed superior performance over state-of-the-art methods on benchmark datasets, becoming the winner of the NTIRE2017 SR Challenge [27].

3.4 Generative Models for Super-Resolution Enhancement

Generative Adversarial Networks (GANs) have been a breakthrough in Single Image Super-Resolution (SISR), starting with the SRGAN [25], which introduced the concept of using a GAN for SR tasks. This model features a generator that creates super-resolved images and a discriminator that distinguishes between real and generated high-resolution images. If the discriminator cannot tell the difference, the generated image is considered a successful approximation of the high-resolution output. The generator in SRGAN is based on the SRResNet model, a residual network comprising five blocks of two conventional layers (Conv-BN-ReLU).

Building on this, the SRFeat [22] model introduces a new generator with long-range hop connections, enabling more efficient transfer of information across distant layers. It also incorporates two types of discriminators: an image discriminator and a feature discriminator, the latter focusing on preserving high-frequency structural features while reducing noise artifacts, enhancing image quality. The ESRGAN [30] model takes SRGAN a step further by significantly improving visual quality. It introduces a generator based on a multi-block Residual in Residual Dense Block (RRDB) architecture, eliminating Batch Normalization (BN) layers for better performance. Additionally, ESRGAN employs a relativistic GAN discriminator, which learns to evaluate the realism of generated images, pushing the generator to recover finer textures and details. This progression demonstrates how each GAN-based model builds on its predecessor, improving the quality of generated super-resolved images by refining the generator and discriminator architectures, while focusing on finer details and better texture representation.

3.5 Comparison of Super-Resolution Models selected from literature

his section provides an overview of several deep learning and generative model-based Super-Resolution (SR) techniques. These models were adapted for CTA images, implemented, evaluated, and analyzed, as they are typically used for biological image processing. A summary of the evaluated models is presented in Table 1,

where each model is categorized based on its architecture and methodology. This classification offers a structured approach to understanding their strengths and capabilities, particularly in addressing the challenges of enhancing vascular structure visualization in CTA images.

Table 1 Comparison of SR Models evaluated for CTA images, based on their network architectures and characteristics.

Model	Convolutional model-based	Residual model-based	GAN model-based
SRCNN915 [5]	X		
SRCNN955 [5]	X		
EDSR [17]	X	X	
RCAN [32]	X	X	
SRGAN [25]	X		X
ESRGAN [30]	X		X

4 Materials and Methods

4.1 Dataset

The data consisted of anonymized CTA medical images of lower extremities in DICOM format [2]. CT imaging, using X-ray radiation, produces anatomical slices for diagnostics [4]. Each image is made of voxels, with values reflecting tissue density on the Hounsfield scale [4]. CTA is used to detect conditions like arterial aneurysms, blockages, blood clots, and PAOD [8].
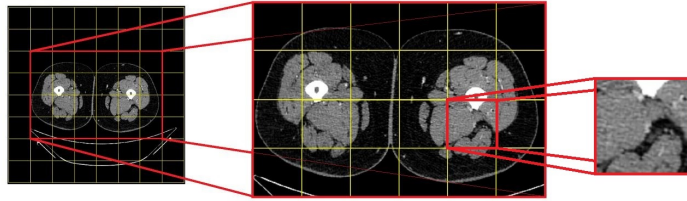
Fig. 2 Cell selection for training and validation. If 600 slices (on average) are selected in a study and from each slice 24 block cells are used, we have about 14,400 64x64 pixel images for training/validation the SR models.

The images obtained by CTA in this study are volumetric data of size 512×512 pixels per slice. Due to the large computational demands of deep learning networks, 64×64 blocks were used for training. The selected block is used as an output image (target), while the input is a bicubic-downsampled version of the same block for testing purpose.

4.2 Image selection

For this study, we selected CTA images of the lower extremities, manually removing the initial and final slices to retain only the relevant images from the genitalia to the

ankle. On average, each study/series included around 600 images, all of which were anonymized. To optimize memory usage during SR model training, we divided each 512x512 pixel slice into smaller 64x64 pixel blocks, preventing memory overflow and ensuring smooth execution. Since many of these blocks did not contain relevant information, we focused only on the most informative cells, as shown in Figure 2.

4.3 Development Tools

Python was used as the programming language, along with various packages that facilitate the implementation of artificial intelligence, including Pandas [1], Numpy [2], TensorFlow [3], Keras [4], sci-kit-learn [5], and OpenCV-python [6]. We tested the algorithms using Jupyter Notebook [7]. For handling DICOM images, we used the Pydicom library [8]. The 3-D modeling of the original studies and those obtained after applying the SR method was performed with 3D-Slicer [9]. This tool is an open-source software designed for the visualization, processing, segmentation, registration, and analysis of 3-D medical, biomedical, and other images and meshes.

4.4 Evaluation metrics

Any processing performed on an image can cause a significant loss of information or quality. Several metrics allow to evaluate such loss. PSNR, related to Mean Square Error (MSE), evaluates the quality of the image reconstruction by numerically comparing the original image and the image generated by the reconstruction [24]; it gives a rough estimate of the human perception of the reconstruction quality. Its measure is in decibels (dB), and its value tends to infinity, so the higher it is, the better the quality of the generated image. On the other hand, a lower PSNR value means a big numerical difference between images. SSIM is a model based on the perception of the human visual system. It measures the similarity between the original and reconstructed image by considering structural information, luminance, and contrast [12]. The SSIM index is a decimal value between -1 and 1, with 0 indicating no structural similarity, 1 indicating a perfectly similar structure, which is achieved in the case of two identical images, and -1 indicate a perfect anti-correlation, meaning the images are structurally opposite [20].

---

[1] https://pandas.pydata.org/

[2] https://numpy.org/

[3] https://www.tensorflow.org/

[4] https://keras.io/

[5] https://scikit-learn.org/stable/

[6] https://opencv.org/

[7] https://jupyter.org/

[8] https://pydicom.github.io/

[9] https://www.slicer.org/

4.5 Super-resolution CNN models applied to CTA images

The success of deep learning in SR has led to the development of numerous methods. In this paper, we compared and adapted various SRCNN models for lower extremity CTA images, using the same loss functions and optimizer as the original authors. We also computed metrics like maximum PSNR [12] and SSIM [20] to quantitatively evaluate the results. Notably, the final convolution layer, responsible for reconstructing the output image, generates a one-dimensional feature map due to the monochrome (single-channel) nature of the CTA images. Below, we describe the architecture of each SR model implemented and evaluated.

Super-resolution convolutional neural network (SRCNN) In 2014, Dong et al. [5] introduce this method. They use a CNN that takes the low-resolution image as input and generates the high-resolution image. The architecture is shown in Fig. 3, it was adapted to CTA images.
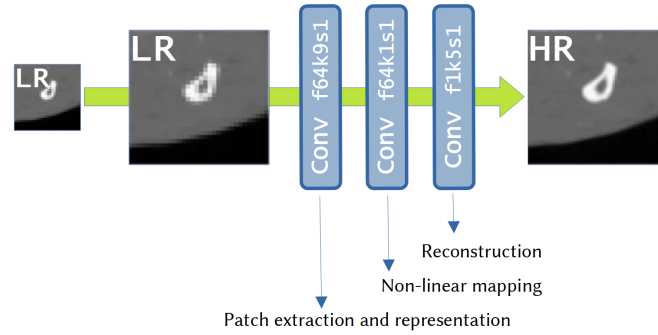
Fig. 3 Implementation scheme of the SRCNN 9-1-5 model. Each convolution is defined by the number of features, the size of the convolution matrix (kernel), and the convolution step (stride).

Initially, the low-resolution image is pre-processed by enlarging it to match the high-resolution image using bi-cubic interpolation. The end-to-end learning consists of three convolutional steps: first, extracting patches from the low-resolution image as high-dimensional vectors; second, performing nonlinear mapping to create feature maps; and third, reconstructing the high-resolution image by aggregating these patch representations. And in 2015, Dong. et. al published version 3 of their paper [5], where they generalize the second step of their method by applying larger filters, thereby achieving better learning results, and designed the SRCNN 9-5-5 model architecture (see Fig. 4).

SRCNN model numbers such as 9-1-5 and 9-5-5 refer to the filter sizes and number of filters used in each convolutional layer. SRCNN 9-1-5 uses a 9x9 filter size in the first layer, a 1x1 filter size in the second layer and a 5x5 filter size in the third layer. On the other hand, SRCNN 9-5-5 uses a filter size of 9x9 in the first layer, a filter size of 5x5 in the second layer and a filter size of 5x5 in the third layer. In

SRCNN 9-5-5
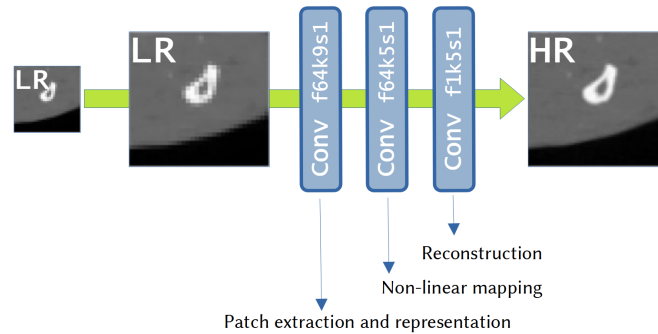
Fig. 4 SRCNN 9-5-5 model architecture.

Figures 3 and 4, codes such as f64k9s1, f64k1s1 describe the configuration of the convolutional layers in terms of filters, core size and stride, for example:

- **f64k9s1**: indicates the convolution layer is composed of 64 filters (f64) with a kernel size of 9x9 (k9), and stride of 1 (s1).
- **f64k1s1**: indicates the convolution layer is composed of 64 filters (f64) with a kernel size of 1x1 (k1), and stride of 1 (s1).

EDSR (ENHANCED DEEP RESIDUAL NETWORK FOR SINGLE IMAGE SUPER-RESOLUTION)
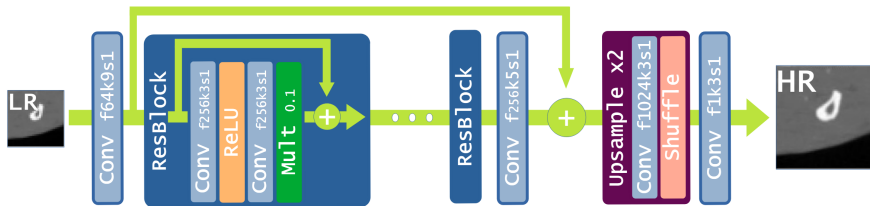
Fig. 5 EDSR model architecture

Enhanced Deep Residual Networks for Single Image Super-resolution (EDSR) Based on SRResNet [25], it consists of a series of ResBlocks followed by an image scaling block, as shown in Fig. 5. Unlike SRResNet, EDSR removes Batch Normalization (BN) layers, improving performance without compromising quality. This allows for deeper networks that outperform conventional Residual Networks (ResNet)[11]. However, training became unstable when feature maps exceeded a threshold, which was addressed by applying a residual scale of 0.1 in each block (shown as 'Mult 0.1' in Fig. 5). The final block scales the image by ×2, with a second block used for ×4 scaling.

Residual Channel Attention Networks (RCAN) [32] It consists of four main components: shallow feature extraction, residual deep feature extraction via Residual-in-Residual (RIR) modules, a scaling module, and a reconstruction module. The

shallow feature extraction uses a single convolutional layer, while the RIR module, composed of multiple Residual Groups (RGs) with Residual Channel Attention Blocks (RCABs), facilitates deep feature extraction. The scaling module, based on ESPCNN [25], improves image resolution. Long hop connections enable the network to focus on key low-resolution features. Additionally, the Channel Attention (CA) mechanism helps the network prioritize informative features by considering channel inter-dependencies. This architecture supports the training of very deep networks, with over 400 layers.
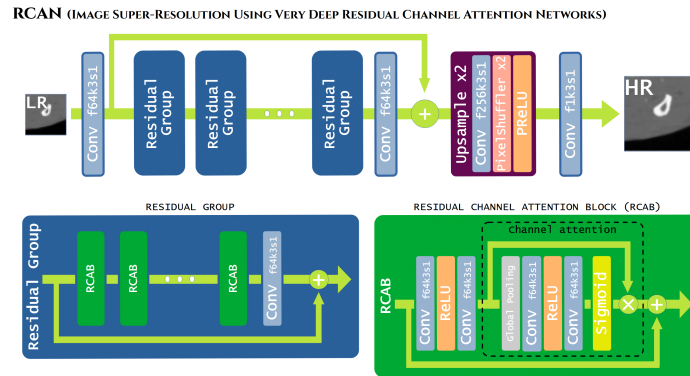
Fig. 6 RCAN model architecture

Super-resolution using GAN (SRGAN) This model aims to improve perceptual quality over traditional PSNR-based methods. While PSNR decreases, the overall structural quality improves, and the goal is to generate SR images with high-quality structures for reliable 3-D reconstruction. In this approach, the focus is on training the generator without adversarial training. The SRGAN [25] generator, known as SRResNet, is a deep residual network that diverges from MSE as the sole optimization objective. The architecture (see Fig. 7) includes 16 residual blocks, each formed by two convolutional layers (3×3) with 64 feature maps, batch normalization, and ParametricReLU (PReLU) activation. The resolution is increased through ×2 scaling blocks using 3×3 convolutions with 256 feature maps, followed by pixel shuffling and PreLU activation. The final output is produced by applying a 3×3 convolution with a single feature map. The 'tanh' activation function, which captures both positive and negative features, yields the best results in super-resolution tasks by preserving high-frequency details.

Enhanced Super-Resolution GAN (ESRGAN): [30] It improves image quality over SRGAN by making two key modifications to the generator: removing Batch Normalization (BN) layers and introducing a new basic block called the Residual in Residual Dense Block (RRDB). The RRDB combines a multilevel residual network with dense connections, as shown in Fig. 8. Removing BN layers enhances performance, improves network adaptability, and reduces computational complexity and memory usage, while also minimizing the risk of artifacts in deep networks. The RRDB structure is more complex than the original SRGAN residual block, featuring a residual-in-residual design that performs residual learning at multiple levels using
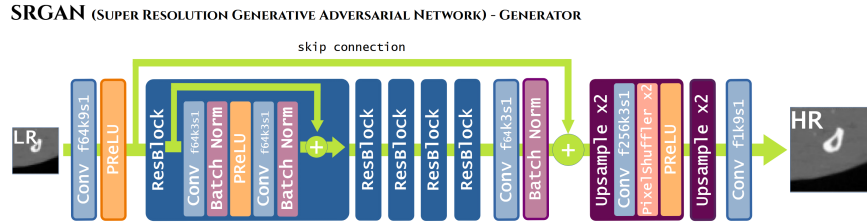
Fig. 7 SRGAN model architecture
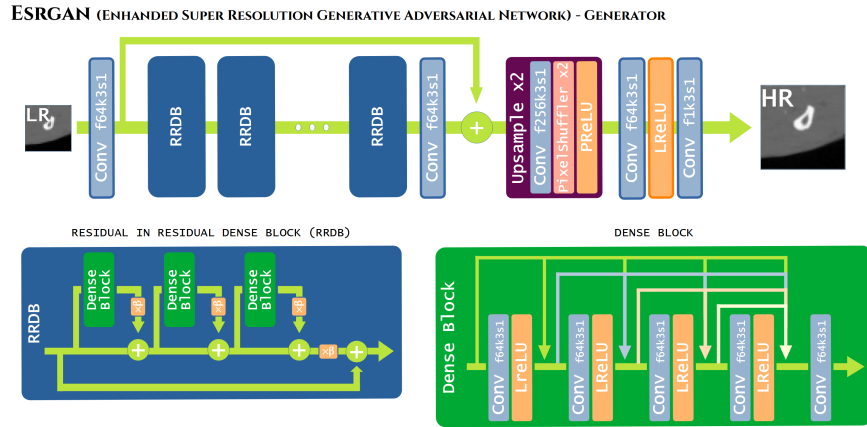
Fig. 8 ESRGAN model architecture.

dense blocks. Additionally, residual scaling, by multiplying by a constant β (between 0 and 1), is applied to prevent instability and improve training stability.

5 Results

In order to perform comparative training between the different models selected in this work, the same set of images was used for all of them. Two CTA studies were used, the first study had 596 slices, and the second had 580 slices. The image selection was performed as specified in section 4.2. Twenty percent (20%) of the slices were used for validation, and the rest were used for training. Each slice provides a batch of 8 images of 64×64 pixels. Finally, using 7,528 images for training and 1,880 images for validation. All models were subjected to a 10-epoch training using the parameters defined by their authors in the published papers.

In the GAN networks only the generator network is trained, since a GAN training with discriminator brings visual realism to the images but introduces artifacts in the image [25, 30], especially in tiny structures, which could affect its use for medical diagnosis [31]. An ×8-scale training was performed for the models (SRCNN 9-5-5)

that our available resources could support. However, the quantitative and qualitative results were so poor that they were not worth presenting.

The bi-cubic interpolation [10] is not a neural network model but a mathematical model used to perform image scaling, and we used it as a reference. Bi-cubic interpolation uses a weighted average of the 16 nearest pixels (4x4 grid) around the target pixel. Table 2 displays the PSNR and SSIM values for scales x2 and x4, from every method studied. The observed trend reveals a decrease in visual quality starting from the ×4 scale, every model showed better results on scale x2.
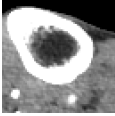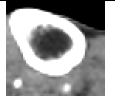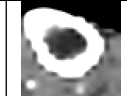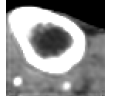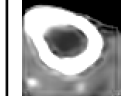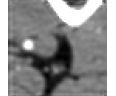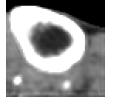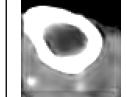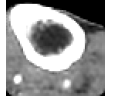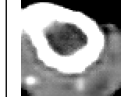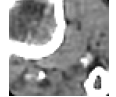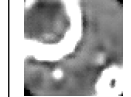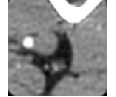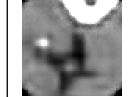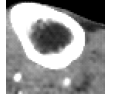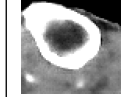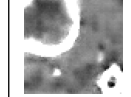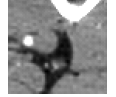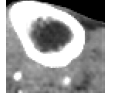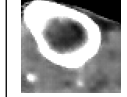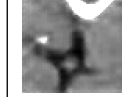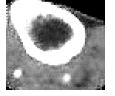
The SRCNN model, characterized by its simplicity with just three convolutions, demonstrates notable performance compared to the other implemented models for this image type. The SRCNN 9-5-5 model, which consists of a 5×5 convolution matrix in the central convolution, performs lighter better than the model SRCNN 9-1-5 (see Table 2). However, it is not possible to say which of them perform better. Although the EDSR model was developed as an enhancement of the SRRestNet model (SRGAN generator), it has exhibited inferior results, particularly at the ×4 scale, where the difference is significantly noticeable both in qualitative and quantitative terms. Please refer to Table 2 for a detailed presentation of the results.

The authors of RCAN defined in their paper a model configuration of 10 RG with 20 RCAB each. However, after testing several configurations in this study, better results have been obtained with 2 RGs and 20 RCABs each. These results are shown in Table 2.

On the other hand, the SRGAN model defines a generator (SRResNet) that has been taken as a reference in the literature due to its quality, especially at scales ×4 or larger. This model with momentum equal to 0.5 in the Batch-Normalization, as used by the creators, the PSNR and SSIM indicated high-quality reconstruction with minimal loss of detail and strong structural similarity to the original image, but generated large artifacts in most of the images for x4 scale and degenerated their 3-D representation. After several tests, we realized that reducing the momentum to 0.2 prevented artifacts at x4 scale and produced better results, though still not as good as the RCAN model. The results obtained in the training of this model reflected in Table 2 showed that on CTA images with the scale x4 it performs better than the scale x2 compared with RCAN model, as we can see in Table 2, but there was not so much difference. However SRGAN is slightly better in the scale x4 than RCAN. SRGAN performed better than the others models compared, including the RCAN, at the scale x4 (see Table 2).

The ESRGAN model is considered by the literature as an improvement of its predecessor SRGAN, using a full GAN (generator-discriminator) training. In this study only the generator of the models is used for reasons already defined, with 64 features and 23 RRDB blocks. In this case we have worse results than its predecessor, as can be seen in Table 2.

Table 2 Summary of the results obtained by the applied methods, with metrics at x2 and x4 scales, tested on the same arterial area, in three different patients

Patient 2		Patient 3		Patient 4	
Original ROI					
x2 scale	x4 scale	x2 scale	x4 scale	x2 scale	x4 scale
BICUBIC					
PSNR 35.93 SSIM 0.9796	PSNR 27.03 SSIM 0.8670	PSNR 35.39 SSIM 0.9746	PSNR 26.37 SSIM 0.8518	PSNR 40.16 SSIM 0.9819	PSNR 32.95 SSIM 0.9415
SRCNN 9-1-5					
PSNR 36.66 SSIM 0.9814	PSNR 28.48 SSIM 0.9305	PSNR 36.20 SSIM 0.9753	PSNR 27.49 SSIM 0.8735	PSNR 40.91 SSIM 0.9813	PSNR 34.53 SSIM 0.9433
SRCNN 9-5-5					
PSNR 35.71 SSIM 0.9786	PSNR 28.23 SSIM 0.8981	PSNR 35.69 SSIM 0.9746	PSNR 27.84 SSIM 0.8831	PSNR 39.48 SSIM 0.9802	PSNR 33.58 SSIM 0.9422
EDSR					
PSNR 37.56 SSIM 0.9868	PSNR 25.70 SSIM 0.8472	PSNR 34.79 SSIM 0.9813	PSNR 24.29 SSIM 0.8362	PSNR 38.22 SSIM 0.9850	PSNR 29.84 SSIM 0.9323
RCAN					
PSNR 41.82 SSIM 0.9903	PSNR 31.55 SSIM 0.9422	PSNR 41.16 SSIM 0.9845	PSNR 29.09 SSIM 0.9107	PSNR 46.21 SSIM 0.9865	PSNR 36.32 SSIM 0.9527
SRGAN					
PSNR 40.85 SSIM 0.9897	PSNR 31.97 SSIM 0.9500	PSNR 40.50 SSIM 0.9846	PSNR 30.18 SSIM 0.9196	PSNR 44.60 SSIM 0.9860	PSNR 36.36 SSIM 0.9537
ESRGAN					
PSNR 35.65 SSIM 0.9789	PSNR 25.45 SSIM 0.8172	PSNR 33.03 SSIM 0.9730	PSNR 25.06 SSIM 0.8166	PSNR 36.65 SSIM 0.9804	PSNR 28.26 SSIM 0.9166

6 Discussion

The compared models allow obtaining better results at PSNR and SSIM level than the mathematical scaling models such as the bi-cubic one. We can observe in Table 2 that, for this type of images with a single channel, at ×2 scale even better results are obtained than with color images, if we consider the results obtained by the authors of the models reflected in the literature [5, 17, 25, 30, 32]. Table 2 shows the results for scale ×2, and x4. The best result for scale x2 was achieved by RCAN model, while the best result for scale x4 were obtained for the SRGAN model. Using the RCAN and SRGAN models, the best SR models compared for ×2 and ×4 scales, respectively, we can test the effect of SR on CTA images of the lower extremities. If we create a 3-D representation of the obtained images, we can observe how the small arteries become more prominent due to the effect of the super-resolution, as shown in Figures 9, 10, and 11. Images are frontal visualization of a 3-D rendering images generated using 3D-Slicer [7], an open source rendering and visualization tools.
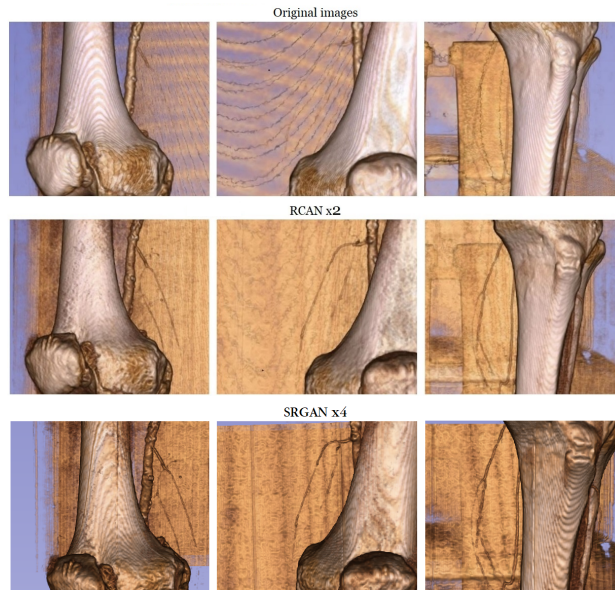
Fig. 9 3-D visualization of the effect of SR (Patient 5). The first row shows the original images, second row shows the best result using the RCAN model at scale x2, and the third row shows the best result using the SRGAN model at scale x4.

7 Conclusion and Future Work

In this study, we addressed the limitations of standard CTA in capturing the detailed morphology of small arteries, particularly in the lower extremities. To overcome this challenge, we applied advanced super-resolution (SR) techniques to enhance the

Fig. 10 3-D visualization of the SR effect (Patient 6), also with best results with RCAN and SRGAN models (x2 ans x4 scale respectively).
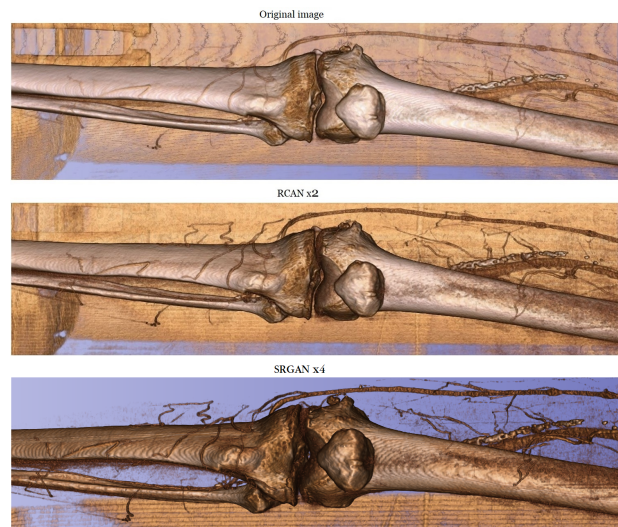
Fig. 11 3-D visualization of the SR effect (Patient 7), also with best results with RCAN and SRGAN models (x2 ans x4 scale respectively).

three-dimensional (3-D) reconstruction and visualization of lower extremity arteries

using standard CTA images. We evaluated various single-image super-resolution (SISR) models tailored for CTA images, including SRCNN, EDSR, RCAN, SRGAN, and ESRGAN. Among them, the RCAN (Residual Channel Attention Networks) and SRGAN (Super-Resolution Generative Adversarial Network) models stood out as the most effective. RCAN excelled at a two-times (x2) scale, while SRGAN performed exceptionally well at a four-times (x4) scale. These models have different objectives, with RCAN focusing on improving high-resolution image quality and SRGAN specialized in up-scaling low-resolution images.

Our findings demonstrate that these SR techniques significantly improved image quality and enabled the visualization of previously indistinct or imperceptible arteries, which holds promise for conditions like peripheral arterial occlusive disease (PAOD). This advancement underscores the role of intelligent systems in enhancing medical diagnostics and decision support. This chapter exemplifies how cutting-edge technologies in artificial intelligence and machine learning can transform healthcare by providing clinicians with powerful tools to analyze complex information and make more informed decisions, showcasing intelligent systems that support decision-making across various fields.

Future research should explore the application of SR methods to enhance inter-slice quality in CTA images, as this could provide additional diagnostic insights into arterial diseases. Despite challenges such as computational cost and time constraints, our study highlights the potential of SR techniques as a valuable tool for diagnosing PAOD. By integrating these advanced techniques into clinical practice, we can improve diagnostic capabilities in vascular imaging, ultimately leading to better decision-making and patient outcomes.

Competing Interests The authors have no conflicts of interest to declare that are relevant to the content of this chapter.

Ethics Approval This study adhered to ethical standards and regulations, utilizing anonymized patient data from the Medical University of Vienna, collected during research between 2002 and 2006. All identifiable information was removed to ensure patient confidentiality and privacy. The anonymization process guaranteed that individual identities could not be traced from the dataset. This research follows the principles of the Declaration of Helsinki, and the use of anonymized data without explicit consent is widely accepted in research when strict anonymization and ethical standards are followed. By prioritizing patient privacy, this study aims to provide valuable insights for both current and future patients.

References

1. Bolaños Martínez, I., Chaves Chaves, A., Gallón Vanegas, L., Ibañez Morera, M., López Barquero, H.: Enfermedad arterial periférica en miembros inferiores. Medicina Legal

de Costa Rica **36**(1), 84–90 (2019)

2. Chin, H., Klepac, D., Ernst, R.D., et al.: Digital photography of digital imaging and communications in medicine—3 images from computers in the radiologist's office. J Digit Imaging (1999)

3. Clement, D.: Medical treatment of peripheral artery occlusive disease (paod). Acta Chirurgica Belgica **100**(5), 190–193 (2000)

4. Costa, J., Soria, J.: Tomografía Computarizada dirigida a Técnicos Superiores en Imagen para el Diagnóstico. Fotoletra, S.A. (2015)

5. Dong, C., Loy, C.C., He, K., Tang, X.: Learning a deep convolutional network for image super-resolution. In: D. Fleet, T. Pajdla, B. Schiele, T. Tuytelaars (eds.) Computer Vision – ECCV 2014, pp. 184–199. Springer International Publishing, Cham (2014)

6. Dong, C., Loy, C.C., Tang, X.: Accelerating the super-resolution convolutional neural network. In: B. Leibe, J. Matas, N. Sebe, M. Welling (eds.) Computer Vision – ECCV 2016, pp. 391–407. Springer International Publishing, Cham (2016)

7. Fedorov, A., Beichel, R., Kalpathy-Cramer, J., Finet, J., Fillion-Robin, J.C., Pujol, S., Bauer, C., Jennings, D., Fennessy, F.M., Sonka, M., Buatti, J., Aylward, S.R., Miller, J.V., Pieper, S., Kikinis, R.: 3d slicer as an image computing platform for the quantitative imaging network. Magnetic Resonance Imaging **30**(9), 1323–1341 (2012)

8. Fleischmann, D., Lammer, J.: Peripheral ct angiography for interventional treatment planning. Eur Radiol Suppl **16**, M58–M64 (2006). DOI 10.1007/s10406-006-0197-y

9. Goodfellow, I., Pouget-Abadie, J., Mirza, M., Xu, B., Warde-Farley, D., Ozair, S., Courville, A., Bengio, Y.: Generative adversarial networks. Commun. ACM **63**(11), 139–144 (2020). DOI 10.1145/3422622. URL https://doi.org/10.1145/3422622

10. Han, D.: Comparison of commonly used image interpolation methods. In: Proceedings of the 2nd International Conference on Computer Science and Electronics Engineering (ICCSEE 2013), pp. 1556–1559. Atlantis Press (2013). DOI 10.2991/iccsee.2013.391

11. He, K., Zhang, X., Ren, S., Sun, J.: Deep residual learning for image recognition. In: 2016 IEEE Conference on Computer Vision and Pattern Recognition (CVPR), pp. 770–778 (2016). DOI 10.1109/CVPR.2016.90

12. Horé, A., Ziou, D.: Image quality metrics: Psnr vs. ssim. In: 2010 20th International Conference on Pattern Recognition, pp. 2366–2369 (2010). DOI 10.1109/ICPR.2010.579

13. Kim, J., Lee, J., Lee, K.: Accurate image super-resolution using very deep convolutional networks. In: 2016 IEEE Conference on Computer Vision and Pattern Recognition (CVPR), pp. 1646–1654. IEEE Computer Society, Los Alamitos, CA, USA (2016). DOI 10.1109/CVPR.2016.182. URL https://doi.ieeecomputersociety.org/10.1109/CVPR.2016.182

14. Kim, J., Lee, J.K., Lee, K.M.: Deeply-recursive convolutional network for image super-resolution. In: 2016 IEEE Conference on Computer Vision and Pattern Recognition (CVPR), pp. 1637–1645 (2016). DOI 10.1109/CVPR.2016.181

15. La Cruz, A., Straka, M., Kochl, A., Sramek, M., Groller, E., Fleischmann, D.: Non-linear model fitting to parameterize diseased blood vessels. In: IEEE Visualization 2004, pp. 393–400 (2004). DOI 10.1109/VISUAL.2004.72

16. Lai, W.S., Huang, J.B., Ahuja, N., Yang, M.H.: Deep laplacian pyramid networks for fast and accurate super-resolution. In: 2017 IEEE Conference on Computer Vision and Pattern Recognition (CVPR), pp. 5835–5843 (2017). DOI 10.1109/CVPR.2017.618

17. Lim, B., Son, S., Kim, H., Nah, S., Lee, K.M.: Enhanced deep residual networks for single image super-resolution. In: 2017 IEEE Conference on Computer Vision and Pattern Recognition Workshops (CVPRW), pp. 1132–1140 (2017). DOI 10.1109/CVPRW.2017.151

18. Nakanishi, R., Motoyama, S., Leipsic, J., Budoff, M.J.: How accurate is atherosclerosis imaging by coronary computed tomography angiography? Journal of Cardiovascular Computed Tomography **13**, 254–260 (2019). DOI 10.1016/j.jcct.2019.06.005

19. Napoli, A., Fleischmann, D., Chan, F.P., Catalano, C., C., H.J., Passariello, R., Rubin, G.D.: Computed tomography angiography. Journal of Computer Assisted Tomography **28**, S32–S45 (2004). DOI 10.1097/01.rct.0000120859.80935.10

20. Ndajah, P., Kikuchi, H., Yukawa, M., Watanabe, H., Muramatsu, S.: Ssim image quality metric for denoised images. In: Proceedings of the 3rd WSEAS International Conference on Visualization, Imaging and Simulation, VIS '10, p. 53–57. World Scientific and Engineering Academy and Society (WSEAS), Stevens Point, Wisconsin, USA (2010)

21. Norgren, L., Hiatt, W., Dormandy, J., Nehler, M., Harris, K., Fowkes, F.: Inter-society consensus for the management of peripheral arterial disease (tasc ii). European Journal of Vascular and Endovascular Surgery **33**(1), S1–S75 (2007). DOI 10.1016/j.ejvs.2006.09.024. Supplement

22. Park, S.J., Son, H., Cho, S., Hong, K.S., Lee, S.: Srfeat: Single image super-resolution with feature discrimination. In: V. Ferrari, M. Hebert, C. Sminchisescu, Y. Weiss (eds.) Computer Vision – ECCV 2018, pp. 455–471. Springer International Publishing, Cham (2018)

23. Preim, B., Oeltze, S.: 3d visualization of vasculature: An overview. In: L. Linsen, H. Hagen, B. Hamann (eds.) Visualization in Medicine and Life Sciences, pp. 39–59. Springer Berlin Heidelberg, Berlin, Heidelberg (2008)

24. Sara, U., Akter, M., Uddin, M.: Image quality assessment through fsim, ssim, mse and psnr—a comparative study. Journal of Computer and Communications **7**, 8–18 (2019). DOI 10.4236/jcc.2019.73002

25. Shi, W., Caballero, J., Huszar, F., Totz, J., Aitken, A.P., Bishop, R., Rueckert, D., Wang, Z.: Real-time single image and video super-resolution using an efficient sub-pixel convolutional neural network. In: 2016 IEEE Conference on Computer Vision and Pattern Recognition (CVPR), pp. 1874–1883. IEEE Computer Society, Los Alamitos, CA, USA (2016). DOI 10.1109/CVPR.2016.207. URL https://doi.ieeecomputersociety.org/10.1109/CVPR.2016.207

26. Tai, Y., Yang, J., Liu, X.: Image super-resolution via deep recursive residual network. In: 2017 IEEE Conference on Computer Vision and Pattern Recognition (CVPR), pp. 2790–2798 (2017). DOI 10.1109/CVPR.2017.298

27. Timofte, R., Agustsson, E., Gool, L.V., et al.: Ntire 2017 challenge on single image super-resolution: Methods and results. In: 2017 IEEE Conference on Computer Vision and Pattern Recognition Workshops (CVPRW), pp. 1110–1121 (2017). DOI 10.1109/CVPRW.2017.149

28. Tong, T., Li, G., Liu, X., Gao, Q.: Image super-resolution using dense skip connections. In: 2017 IEEE International Conference on Computer Vision (ICCV), pp. 4809–4817 (2017). DOI 10.1109/ICCV.2017.514

29. Uhl, J.F., Prat, G., Costi, D., Ovelar, J.A., Scarpelli, F., Ruiz, C., Lorea, B.: Modelado 3d del sistema vascular. Flebología **44**, 17–27 (2018)

30. Wang, X., Yu, K., Wu, S., Gu, J., Liu, Y., Dong, C., Qiao, Y., Loy, C.C.: Esrgan: Enhanced super-resolution generative adversarial networks. In: L. Leal-Taixé, S. Roth (eds.) Computer Vision – ECCV 2018 Workshops, pp. 63–79. Springer International Publishing, Cham (2019)

31. You, C., Cong, W., Vannier, M.W., Saha, P.K., Hoffman, E.A., Wang, G., Li, G., Zhang, Y., Zhang, X., Shan, H., Li, M., Ju, S., Zhao, Z., Zhang, Z.: CT super-resolution GAN constrained by the identical, residual, and cycle learning ensemble (GAN-CIRCLE). IEEE Transactions on Medical Imaging **39**(1), 188–203 (2020). DOI 10.1109/tmi.2019.2922960

32. Zhang, Y., Li, K., Li, K., Wang, L., Zhong, B., Fu, Y.: Image super-resolution using very deep residual channel attention networks. In: V. Ferrari, M. Hebert, C. Sminchisescu, Y. Weiss (eds.) Computer Vision – ECCV 2018, pp. 294–310. Springer International Publishing, Cham (2018)

33. Zhang, Y., Tian, Y., Kong, Y., Zhong, B., Fu, Y.: Residual dense network for image super-resolution. In: 2018 IEEE/CVF Conference on Computer Vision and Pattern Recognition, pp. 2472–2481 (2018). DOI 10.1109/CVPR.2018.00262

34. Zhou, L., Fan, M., Hansen, C., Johnson, C.R., Weiskopf, D.: A review of three-dimensional medical image visualization. Health Data Science **2022**, 9840519 (2022). DOI 10.34133/2022/9840519. URL https://spj.science.org/doi/abs/10.34133/2022/9840519

35. Zhu, H., Xie, C., Fei, Y., Tao, H.: Attention mechanisms in cnn-based single image super-resolution: A brief review and a new perspective. Electronics **10**(10) (2021). DOI 10.3390/electronics10101187. URL https://www.mdpi.com/2079-9292/10/10/1187